International Journal Of Industrial Electronics Control and Optimization
Print ISSN: 3517-2645
Online ISSN: 3568-2645
Homepage: https://ieco.usb.ac.ir/

Novel Non-Linear Control of DFIG and SSSC for Stability Increment of Power System

Saeed Abazari

Faculty of Engineering, Shahrekord University, Shahrekord, Iran.
Corresponding author's email: abazari-s@eng.sku.ac.ir

Article Info

Article type:
Research Article

Article history:
Received: 29-May-2023
Received in revised form: 4-Agust-2023
Accepted: 2-December-2023
Published online: 14- Jan-2024

Keywords:
Stability,
Terminal sliding mode,
Sliding mode observer,
DFIG.

ABSTRACT

This study examines stability improvement of the power system which includes Double Feed Induction Generators (DFIGs) and Static Series Synchronous Compensator (SSSC). The proposed nonlinear controller is designed based on the terminal sliding mode control theory. A sliding mode observer is also developed to remove the need to access the information of all the state variables. The final closed-loop of the power system modeling is robust against parameter variations and uncertainties. The limitations of the control signals in the process of controller design are also considered. The application of such a method increases the stability margins and results in higher robustness degrees. A comparison with other nonlinear approaches such as back-stepping and feedback linearization approaches is carried out. The results show the faster and more reliable convergence rate of the power system-controlled trajectories to reach back to the equilibrium point after occurring a sudden fault. The results are obtained by performing a simulation on the standard 39-Bus, 10 machines NEW ENGLAND power system.

Nomenclature

δ_i	Rotor angle of the ith generator
ω_i	Rotor speed of the ith generator
$\acute{E}_{qi}$	Internal voltage of ith generator in q-axes
$\acute{E}_i$	Internal voltage of the ith generator
I_{di}	Stator current of the ith generator in d-axis
I_{qi}	Stator current of the ith generator in q-axis
v_{fi}	Excitation voltage of the ith generator
M_i	Moment of inertia of the ith generator
P_{mi}	Mechanical input power of the ith generator
u_d	Signal control of DFIG
δ_{0i}	Rotor angle of the ith generator in steady state
ω_{0i}	Rotor speed of the ith generator in the steady state
V_i	Amplitude of the ith generator terminal voltage
X_i	Equivalent reactance of DFIG in steady state
θ_i	Phase of the ith generator terminal voltage
$\acute{T}_{d0i}$	Time-constant of the ith generator excitation coil
x_{di}	d-axis steady state reactance of the ith generator
$\acute{x}_{di}$	d-axis transient state reactance of the ith generator
x_{qi}	q-axis steady state reactance of the ith generator

Publisher: University of Sistan and Baluchestan

I. Introduction

The consumption of electrical energy is increasingly growing in today's industrial world. The need for more electrical energy brings attention and widespread investment in building new electrical transmission lines and power plants. The problems of environmental-friendly and safety of the newly built power plants have also been a major factor in generating electrical energy. Paying attention to decreasing the amount of consumption of fossil fuels and pollutant and greenhouse gases in traditional electrical power plants have paved the way to replace them with solar or wind power generation. Due to the emerging technological growth and suitable infrastructure, building wind-turbine power plants has gained a tremendous amount of attention now. In Germany and France, the nuclear power plants are rapidly replacing with wind-turbine ones. For instance, in Germany, five-gigawatt nuclear power plants are replaced with a thousand wind-turbine plants by implementing DFIGs [1].

The second factor in the electrical energy industry is the high cost of constructing new transmission lines to transmit and distribute electrical power. The increase in power energy consumption with the natural limitation of the current transmission networks brings about the problems of insulation, stability, and thermal capacity, [2-3]. Hence, there is a need to distribute the maximum possible power through the available electrical networks. Flexible AC Transmission systems (FACTS) are now spread and installed in electrical networks as a solution to increase transmission capacity. One of the important FACTS components is SSSC, [4-6]. In the SSSC structure, passive elements are not employed. High level of switching mode in SSSC results in the injection and absorption of active electrical power at low cost and high speed.

Maintaining the stability of power networks after occurring a sudden fault is one of the important issues in Transient Stability Assessment (TSA). Moreover, the power system should also be robust against unwanted disturbances. Utilizing DFIGs in addition to SSSC to increase the stability and endurance of power networks is now a major research trend. Applying a suitable control on DFIGs, SSSCs and excitation circuits of synchronous generators will lead to stability improvement [7-10].

In most of the existing research in improving the stability of power networks, power system stabilizers are developed based on a local linear model around the operating point, [11, 12]. In this research area, Linear Matrix Inequalities (LMIs) or Root-Locus methods are implemented to design a linear control law that stabilizes the system all around the operating point. However, power systems are complex nonlinear systems with a high amount of coupling between their components. They are always under enormous power demand to be supplied. Therefore, the operating point varies with different conditions [13]. Hence, assuming local linear models about the operating point and designing local linear control laws result in a closed-loop control system with very low stability margins. Naturally, some researchers have paid attention to implementing nonlinear control laws to design power system stabilizers. For instance, the feedback linearization method by output feedback is implemented in [14] to improve stability with respect to linear control laws. However, in this approach, the exact system model is required to be known. However, usually, there is a need to access high-order derivatives of the signals. Hence, applying this linearization method is very limited in many cases. In [15], linearization by output-feedback is offered, in which, the designer should access the information of all the state variables of the system. Moreover, this method is not robust against parameter variations and structured uncertainties. In the literature survey [16-18], adaptive control techniques for parameter estimation were implemented. These methods have a higher robustness degree with respect to the above-mentioned approaches. However, information on all state variables of the system is needed to be available in the design methodology. In [19, 20], adaptive backstepping approaches are developed to cope with the above difficulties in the design of the nonlinear control laws. However, in this design trend, the coupling effect of SSSC and DFIG are not equally employed to improve stability. Moreover, these methods are again not completely robust performance compared to the existing structured uncertainty in the power system.

In [21-22], adaptive backtracking and multi-input DSC are used to improve stability in which the design of the controller is limited by the number of inputs and outputs. In [23], the transient energy function (TEF) is used. The main problem of using TEFs is the complexity of the controller design for large networks.

In this paper, a terminal sliding mode approach is proposed to enhance the performance of the power system in presence of both DFIG and SSSC. In this regard, by control of the DC link voltage profile, DFIG modeling is considered as a synchronous generator. Besides, another sliding mode observer is also implemented in the design procedure to remove the need to access the information of all the state variables of the system. The close-loop observer-based controller is proved to be stable. In the proposed method, certain existing limitations on the signals in the system are also considered in the design stage. The application of such a method increases stability margins and results in higher robustness degrees.

This paper is organized as follows: In Section 2, a brief review of the power system modeling which includes both DFIG and SSSC is presented. Section 3 until 7is devoted to the design procedure of the proposed control law by applying a terminal sliding mode in addition to a sliding mode observer. In this section, particular attention is paid to the implementation of the designed controller and observer. In Section 8 a simulation is performed to investigate the application of the proposed controller on the specific power network. Also, a comparison is made with the existing results in the literature.

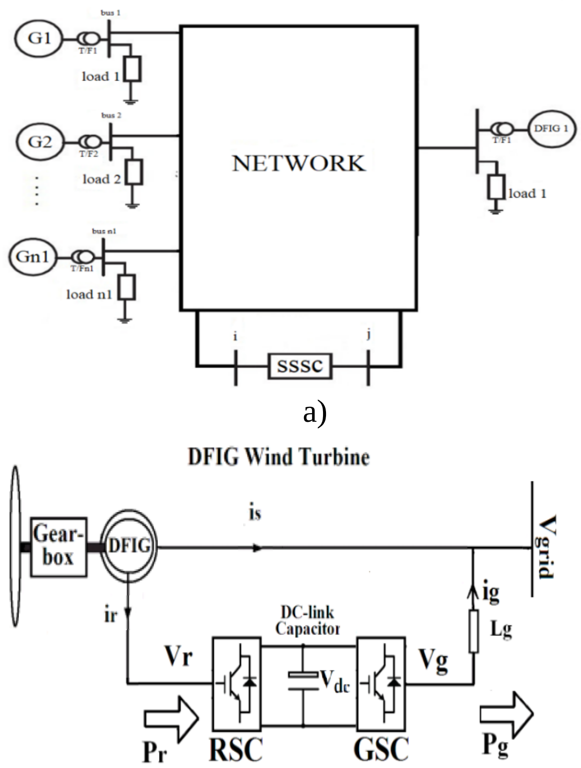

b)

Fig. 1. a) The schematic diagram of the considered case study, b) the diagram of DFIG.

II. Power System Modeling

Fig. 1 depicts the general form of the evaluated power system and the case study. The considered power system consists of n1 synchronous generators, one DFIG component plus one SSSC. It is assumed that the transmission lines resistances are negligible. Hence, the transmission lines are modeled only by $\overline{Y}_{ij} = jB_{ij}$. In the formulation of the power system model, the mechanical power input to the generators is assumed to be constant. Moreover, the resistance of stators is negligible. The total consumed power in each bus is modeled by $Y_i = G_i - jB_i$ [24]. The following mathematical model describes the multi-machine power system including DFIG and SSSC where, V_i و θ_i are the amplitude and phase angle of the connected bus voltage, respectively.

$$\begin{cases} \dot{\delta}_i = \omega_i - \omega_{0i} \\ \dot{\omega}_i = \dfrac{1}{M_i}\left[P_{mi} - \dfrac{\acute{E}_{qi} V_i \sin(\delta_i - \theta_i)}{\acute{x}_{di}} - \dfrac{{V_i}^2 sin2(\delta_i - \theta_i)}{2x_{qi}\acute{x}_{di}}\right] \\ \dot{\acute{E}}_{qi} = \dfrac{1}{\acute{T}_{d0i}}\left(v_{fi} - \dfrac{\acute{E}_{qi} x_{di}}{\acute{x}_{di}} - \dfrac{V_i(x_{di} - \acute{x}_{di})\cos(\delta_i - \theta_i)}{\acute{x}_{di}}\right) \end{cases} \quad (1-a)$$

$$\begin{cases} \dot{\delta}_i = \dfrac{1}{\acute{E}_i T_{0i}}[-T_{0i}(\omega_i - \omega_0)\acute{E}_i - \\ \quad \dfrac{X_i - \acute{X}_\iota}{\acute{E}_{qi} T_{0i}} V_i \sin(\delta_i - \theta_i) + T_{0i}\omega_0 u_{di} \cos(\delta_i)] \\ \dot{\omega}_i = \dfrac{\omega_0}{2H_i}\left[P_{mi}\dfrac{\omega_s}{\omega_i} - B_i \acute{E}_i V_i \sin(\delta_i - \theta_i)\right] \\ \dot{\acute{E}}_i = \dfrac{1}{T_{0i}}\left[-\dfrac{X_i}{\acute{X}_\iota}\acute{E}_i + \dfrac{X_i - \acute{X}_\iota}{\acute{X}_\iota} V_i \cos(\delta_i - \theta_i) + T_{0i}\omega_0 u_{di} \sin(\delta_i)\right] \\ \dot{V}_{dc} = \dfrac{1}{C_{dc} V_{dc}}\left[P_r - \dfrac{1}{x_g}(u_{g2} cos(\theta_i) - u_{g1} sin(\theta_i))\right] \end{cases} \quad (1-b)$$

$$\begin{cases} \dot{V}_i = \sum_{j=1}^{n+p} c_{ij} H_j + \sum_{j=1}^{n+p} d_{ij} v_{fj} + \sum_{j=1}^{n+p} k_{ij}\, r \\ \dot{\theta}_i = \sum_{j=1}^{n+p} c_{i+n+2,j} H_j + \\ \quad \sum_{j=1}^{n+p} d_{i+n+2,j} v_{fj} + \sum_{j=1}^{n+p} k_{i+n+2,j}\, r \end{cases} \quad (1-c)$$

where Eq. (1-a) is related to the synchronous generators. In this study, governor modeling is not considered as it creates a time delay in the stability study. Eq. (1-b) models the DFIG, and Eq. (1-c) describes the bus voltages of the connected buses to the DFIG, SSSC, and synchronous generators. In the above model, v_{fi} (excitation voltage of synchronous generators) represents the control input in the generator excitation circuit, u_{di} is the control input of the RSC part of DFIG, and r is the control signal in the SSSC component [25-26]. Eq. (1-b) models the DFIG. In this equation, $\acute{E}_i$ is the internal voltage of the ith generator, B_i is the reactance of the admittance matrix of the system between the DFIG and its connected bus. Also, $u_{di} = V_{ri} cos(\Phi_{ri})$ is the applied voltages to the DFIG rotor, where V_{ri} and Φ_{ri} are amplitude and phase in polar coordinates, respectively. Due to the structure of back-to-back DFIG converters and the presence of a relatively large capacitor in the DC link, if a suitable controller is not used, it can lead to an adverse effect on the stability of the system. Here, the dynamics of capacitor voltage changes are also considered in the equations. Full details and how to obtain Eq. (1) are given in Appendix A. Eq. (1-c) formulates the relations between the amplitudes and phases of the synchronous generators, the DFIG, and the SSSC with its connected buses. The mathematical Eq. (1) is derived based on the algebraic power balance equations at buses which synchronous generators, DFIG and SSSC are connected to. It is assumed that the SSSC component only generates and consumes reactive power, and its series reactance is zero [27].

Here, considering that the SSSC only produces and absorbs reactive power, the voltage of the capacitor voltage component related to the SSSC has insignificant changes practically, and for this reason, its dynamics have been neglected.

III. Design of terminal sliding mode nonlinear control law

According to Eq. (1), the goal is to convert the equations into the form of state Eq. (2) and to design the terminal sliding controller. Let's consider the n[th]-order nonlinear strict feedback with uncertainty d in the following form:

$$\begin{aligned} &\dot{x}_1 = x_2 \\ &\dot{x}_2 = x_3 \\ &\dot{x}_3 = x_4 \\ &\dots \\ &\dot{x}_{n-1} = x_n \\ &\dot{x}_n = F(x_1, x_2, .., x_n) + G(x_1, x_2, .., x_n)u \\ &\qquad + d(x_1, x_2, .., x_n) \end{aligned} \tag{2}$$

where $x_i \in$ R is the i[th] element of the state-vector for i=1, 2, …, n, and d represents the uncertainty in the system model with the upper bound D>0, F , G are differentiable n-th order with $G \neq 0$, and u∈ R is the control input. Let's define a sliding surface in the following form:

$$S = x_3 + c_2 x_2 |x_2|^{\alpha_2} \mathrm{sgn}(x_2) + c_1 x_1 |x_1|^{\alpha_1} \mathrm{sgn}(x_1) \tag{3}$$

In the above, c_1 و c_2 are constant design factors and α_1 و α_2 satisfy the condition:

$$\begin{cases} 0 < \alpha_2 < 1 \\ \alpha_1 = \dfrac{\alpha_2}{2 - \alpha_2} \end{cases} \tag{4}$$

The sliding surface of (3) can be also written as:

$$S = x_3 + c_2 x_2^{\alpha_2} + c_1 x_1^{\alpha_1} \tag{5}$$

In the sliding condition, $S = 0$, we have:

$$\begin{aligned} &S = x_3 + c_2 x_2^{\alpha_2} + c_1 x_1^{\alpha_1} = 0 \\ &\to x_3 = -c_2 x_2^{\alpha_2} - c_1 x_1^{\alpha_1} \end{aligned} \tag{6}$$

Therefore, (2) and (6) lead to

$$\begin{cases} \dot{x}_1 = x_2 \\ \dot{x}_2 = -c_2 x_2^{\alpha_2} - c_1 x_1^{\alpha_1} \end{cases} \tag{7}$$

Note that c_1 and c_2 are positive scalars that should be designed in such a way that the polynomial $p^2 + c_2 p + c_1$ becomes a Hurwitz polynomial. This fact guarantees that the equilibrium point is stable, and it converges in a limited time. See [28] for complete proof. Differentiating Eq. (6) and Eq. (2) results in the following control law:

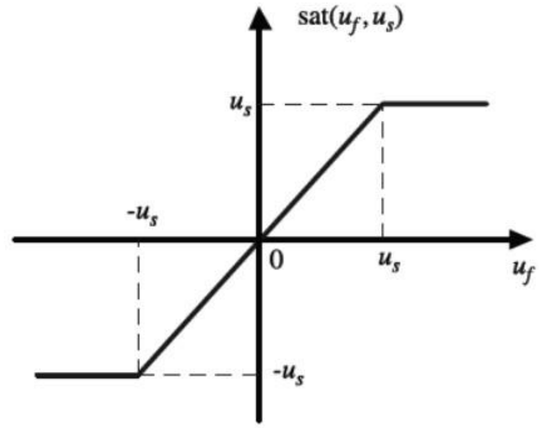

Fig. 2. Saturation function.

$$u = b^{-1}(x)\left[-f(x) + sat(u_f, u_s) - k sgn(s)\right] \tag{8}$$

$$u_f = -c_2 \alpha_2 x_2^{\alpha_2 - 1} x_3 - c_1 \alpha_1 x_1^{\alpha_1 - 1} x_2 \tag{9}$$

In the above, $sat(u_f, u_s)$ is the saturation function depicted in the below figure:

The assumed condition leads to choosing $k = D + \eta$ and constant $\eta > 0$ with $u_s > 0$ as the threshold value.

IV. Implementing the terminal sliding control design to power system

To apply the theory of the terminal sliding mode technique to the power system described by Eq. (1), first, it is essential to define a new set of variables [29]:

$$\begin{cases} x_{1i} = \delta_i - \delta_{i0} \\ x_{2i} = \omega_i - \omega_{0i} \\ \qquad x_{3i} = \dfrac{1}{M_i}\left[P_{mi} - \dfrac{\acute{E}_{qi} V_i \sin(\delta_i - \theta_i)}{\acute{x}_{di}} - \dfrac{V_i^2 \sin 2(\delta_i - \theta_i)}{2 x_{qi} \acute{x}_{di}}\right] \\ \qquad\qquad 1 < i < n_1 \\ \qquad x_{3i} = \dfrac{1}{M_i}\left[P_{mi} \dfrac{\omega_s}{\omega_i} - B_i \acute{E}_i V_i \sin(\delta_i - \theta_i)\right] \\ \qquad\qquad n_1 + 1 < i < n \end{cases} \tag{10}$$

Due to the existing difference between the speed of synchronous generators and DFIG, x_{3i} is introduced in a different form.

The variables of Eq. (10) are strictly defined to achieve a suitable feedback model. Here, x_{1i} is the error related to the internal angle of the generator and the optimal value of the internal angle before the fault occurs for the i-th machine, x_{2i} is the error of the rotor speed compared to the synchronous speed, and x_{3i} is the difference value between the output power and the output of the i-th machine. Because the studied synchronous generators are of the salient pole type and the DFIG generator is of the flat-pole type, the definition of synchronous generators and The DFIG generator is different. Applying the new set of variables in Eq. (1):

$$\begin{cases} \dot{x}_{1i} = x_{2i} \\ \dot{x}_{2i} = x_{3i} \\ \dot{x}_{3i} = f_{Ti} + \sum_{j=1}^{n+2} g_{Tij} v_{fj} + \sum_{j=1}^{n+2} L_{ij}\, r \end{cases} \tag{11}$$

The above equations will transform to the following matrix form version:

$$\begin{cases}\dot{X}_1 = X_2 \\ \dot{X}_2 = X_3 \\ \dot{X}_3 = F_T + G_T V_f + Lr\end{cases} \quad (12)$$

where:

$$V_f = [v_{f1}\ \ v_{f2}\ \ ..\ \ v_{fn-1}\ u_d\ ]^T$$
$$X_1 = [x_{11}\ \ x_{12}\ \ ..\ \ x_{1n}]^T,$$
$$X_2 = [x_{21}\ \ x_{22}\ \ ..\ \ x_{2n}]^T$$
$$,X_3 = [x_{31}\ \ x_{32}\ \ ..\ \ x_{3n}]^T \quad (13)$$

Now, according to Eq. (12), a new control input of the form $U = G_T V_f + Lr$ is defined. This new control input consists of n+1 components.

$U = [u_1\ \ u_2\ \ ..\ \ u_{n+1}]^T$.

In the final stage, with the definition of the sliding surface of the form:

$$s_i = x_{3i} + c_{2i}{x_{2i}}^{\alpha_{2i}} + c_{1i}{x_{1i}}^{\alpha_{1i}} \quad (14)$$

The control inputs will be obtained as:

$$u_i = [-f_i(X) + sat(u_{fi}, u_{si}) - k_i sgn(s_i)] \qquad u_{fi} = \quad (15)$$
$$-c_{2i}\alpha_{2i}{x_{2i}}^{\alpha_{2i}-1}x_3 - c_{1i}\alpha_{1i}{x_{1i}}^{\alpha_{1i}-1}x_{2i} \quad (16)$$

According to Figure 2, the use of the saturation function causes a significant reduction in the output chattering phenomenon .

V. Design of the sliding mode observer

In the power system described by Eq. (1), the angle of each generator rotor and the amplitudes and phases of the terminal voltages of all the generators are accessible for controller design. However, the designer does not access the information on the remaining state variables. Therefore, an observer is needed to estimate these variables. In this paper, a sliding mode observer is proposed. The nonlinear system in Eq. (3) which has only one output is considered in the following way [30-31]:

$$\begin{cases}\begin{pmatrix}\dot{x}_1 \\ \dot{x}_2 \\ \cdot \\ \vdots \\ \dot{x}_{n-1} \\ \dot{x}_n\end{pmatrix} = \begin{pmatrix} x_2 + g_1(x_1, u) \\ x_3 + g_2(x_1, x_2, u) \\ \cdot \\ \vdots \\ x_n + g_{n-1}(x_1, x_2, \dots, x_{n-1}, u) \\ f_n(x, u) + g_n(x, u)\end{pmatrix} \\ y = x_1\end{cases} \quad (17)$$

where x_i represents the state variables, $u \in R^m$ is the control input and $y \in R$ is the only output. f_i and g_i are nonlinear analytical functions. It is possible to introduce the following sliding mode observer:

$$\begin{cases}\begin{pmatrix}\dot{\hat{x}}_1 \\ \dot{\hat{x}}_2 \\ \cdot \\ \vdots \\ \dot{\hat{x}}_{n-1} \\ \dot{\hat{x}}_n\end{pmatrix} = \\ \begin{pmatrix} \hat{x}_2 + g_1(x_1, u) + \lambda_1 sgn_1(\bar{x}_1 - \hat{x}_1) \\ \hat{x}_3 + g_2(x_1, \bar{x}_2, u) + \lambda_2 sgn_2(\bar{x}_2 - \hat{x}_2) \\ \cdot \\ \vdots \\ \hat{x}_n + g_{n-1}(x_1, \bar{x}_2, \dots, \bar{x}_{n-1}, u) \\ +\lambda_{n-1} sgn_{n-1}(\bar{x}_{n-1} - \hat{x}_{n-1}) \\ f_n(x_1, \bar{x}_2, \dots, \bar{x}_n, u) + g_n(x_1, \bar{x}_2, \dots, \bar{x}_n, u) \\ +\lambda_n sgn_n(\bar{x}_n - \hat{x}_n)\end{pmatrix} \\ \hat{y} = \hat{x}_1\end{cases} \quad (18)$$

In the above, $\bar{x}_i$ is defined as:

$$\bar{x}_i = \hat{x}_i + \lambda_{i-1} sgn_{moy,i-1}(\bar{x}_i - \hat{x}_i) \quad (19)$$

where $sgn_{moy,i-1}$ is, in fact, the sgn_{i-1} which is in series with a low-pass filter to transform the saturate function from the initial discontinuous switching function. The function sgn_i is defined below:

$$sgn_i(\bar{x}_i - \hat{x}_i) = $$
$$\begin{cases} 0 \quad \text{, if exists } j \in \{1, .., i-1\} \\ \qquad \text{Such as } \bar{x}_j - \hat{x}_j \neq 0 \\ sgn(\bar{x}_i - \hat{x}_i) \text{ , other}\end{cases} \quad (20)$$

Due to the presence of the sgn term in the state observer modeling, there is chattering in the observed states, and considering that the saturation function is used in the main non-linear controller, the presence of chattering in the observer states does not have much effect on the performance of the controller. In fact, the above function implies that the correcting term becomes active, if and only if for all $j \in \{1, .., i-1\}$, we have $\bar{x}_j - \hat{x}_j = 0$. The λ_i coefficients determine the required convergence time for the observer.

In order to prove the convergence of the proposed observer, it is first assumed that $e_i = x_i - \hat{x}_i$. This assumption implies that $e_1 = x_1 - \hat{x}_1$and

$$\dot{e}_1 = e_2 - \lambda_1 sgn(e_1) \quad (21)$$

Considering $e_2 = \bar{x}_2 - \hat{x}_2$, if $|e_2|_{max} < \lambda_1$, then the sliding surface $e_1 = 0$ will be an attracting surface that can be reached in t_1 time, which leads to $\dot{e}_1 = 0$. Now, a continuous function with the name of $sgn_{eq}$is defined in such a way that $e_2 - \lambda_1 sgn_{eq}(e_1) = 0$. This fact results in $\bar{x}_2 = x_2$. We also have $sgn_{eq} = sgn_{moy}$, therefore,

$$\dot{e}_1 = x_2 - \left(\hat{x}_2 + \lambda_1 sgn_{eq}(x_1 - \hat{x}_1)\right) = \bar{x}_2 - x_2 = 0 \quad (22)$$

Hence, it is obtained that $g_2(x_1, x_2, u) - g_2(x_1, \bar{x}_2, u) = 0$. In this stage, for e_2, we have $\dot{e}_2 = e_3 - \lambda_2 sing(e_2)$. Similar to the above procedure, if one has $|e_3|_{max} < \lambda_2$, then after passing a limited t_2 time, $e_1 = e_2 = 0$ and $\dot{e}_2 = 0$, which both leads to

$\bar{x}_3 = x_3$, and

$$\dot{e}_2 = x_3 - \left(\hat{x}_3 + \lambda_2 sgn_{eq}(x_2 - \hat{x}_2)\right) = \bar{x}_3 - x_3 = 0 \quad (23)$$

Continuing the similar path for the $n-1$ stage, $e_1 = e_2 = .. = e_{n-1} = 0$, which concludes $\bar{x} = x$ in passing t_{n-1} time, the error vector between the actual states and the observed ones converges to zero.

VI. Implementing the sliding observer for the power system including both the DFIG and SSSC

Considering the above procedure in the observer design and Eq. (1), it will be obtained that:

$$\begin{cases} \begin{pmatrix} \dot{X}_1 \\ \dot{X}_2 \\ \dot{X}_3 \end{pmatrix} = \begin{pmatrix} X_2 \\ X_3 \\ F_T + U \end{pmatrix} \\ Y = X_1 \end{cases} \tag{24}$$

where Y is the system output, i.e. the angle of the synchronous generator rotors and the DFIG. According to the above equations, the sliding mode observer will be defined as below:

$$\begin{cases} \begin{pmatrix} \dot{\hat{X}}_1 \\ \dot{\hat{X}}_2 \\ \dot{\hat{X}}_3 \end{pmatrix} = \begin{pmatrix} \hat{X}_2 + \lambda_1 \mathrm{sing}_1(X_1 - \hat{X}_1) \\ \hat{X}_3 + \lambda_2 \mathrm{sing}_2(\bar{X}_2 - \hat{X}_2) \\ F_T(\bar{X}) + U(\bar{X}, u) + \lambda_3 \mathrm{sing}_3(\bar{X}_3 - \hat{X}_3) \end{pmatrix} \\ Y = X_1 \end{cases} \tag{25}$$

and

$$\begin{pmatrix} \bar{X}_1 \\ \bar{X}_2 \\ \bar{X}_3 \end{pmatrix} = \begin{pmatrix} \hat{X}_1 + \lambda_0 \mathrm{sing}_{moy,0}(X_1 - \hat{X}_1) \\ \hat{X}_2 + \lambda_1 \mathrm{sing}_{moy,1}(\bar{X}_2 - \hat{X}_2) \\ \hat{X}_3 + \lambda_2 \mathrm{sing}_{moy,2}(\bar{X}_3 - \hat{X}_3) \end{pmatrix} \tag{26}$$

The control input U is an input vector that includes the of synchronous generators excitation voltage and the controllable voltage of the rotor side converter and the control input related to SSSC. Details on how to apply inputs are given in Appendix A.

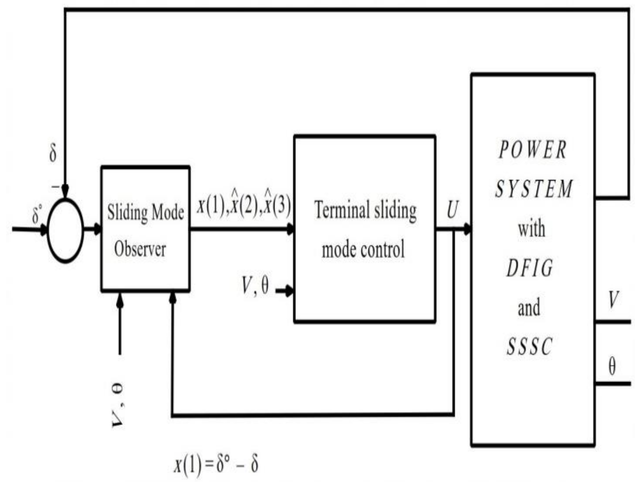

Fig. 3. The Diagram of the proposed terminal sliding mode controller alongside with the observer for the considered power system which includes both DFIG and SSSC.

VII. The proposed algorithm for stability improvement of the power system including the DFIG and SSSC

In the following flowchart, the general configuration for the power system under consideration, applying the terminal sliding mode control law plus a sliding mode observer, is presented.

VIII. Simulation results

To evaluate and validate the effectiveness and performance of the proposed observer-based controller laws on a power system, a simulation is carried out. The considered power system is the standard 39-Bus NEW ENGLAND network. This power system includes 10 synchronous machines, a DFIG component in Bus 19, and a SSSC one between 16, and 19 Buses. The system specifications are presented in Appendix B and a more complete description is offered in [32]:

All simulations are done in the MATLAB software environment.

It is assumed that in the vicinity of G4 of the mentioned power system, a short-circuit fault occurred and lasted for 100 milliseconds. In the first stage, it is assumed that there is no control in the power system. The plot of speed deviation of the G4 generator and DFIG is depicted in Fig. 6-a. As it is observed from this plot, the power system is all unstable.

Fig. 3 depicts the schematic diagram of the systems' performance together with the applied proposed control law:

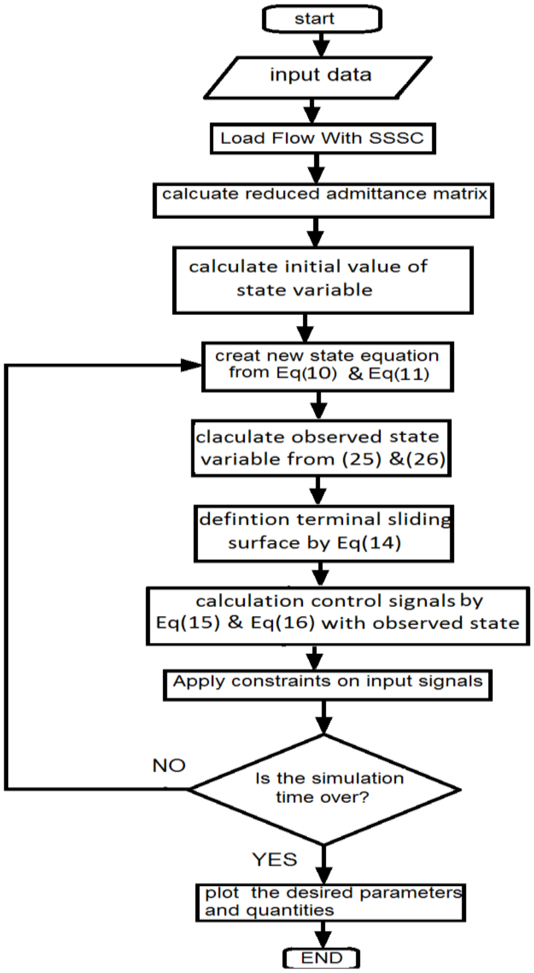

Fig. 4 The simulation flowchart of the power system including both DFIG and SSSC, applying terminal sliding mode control law and the sliding observer.

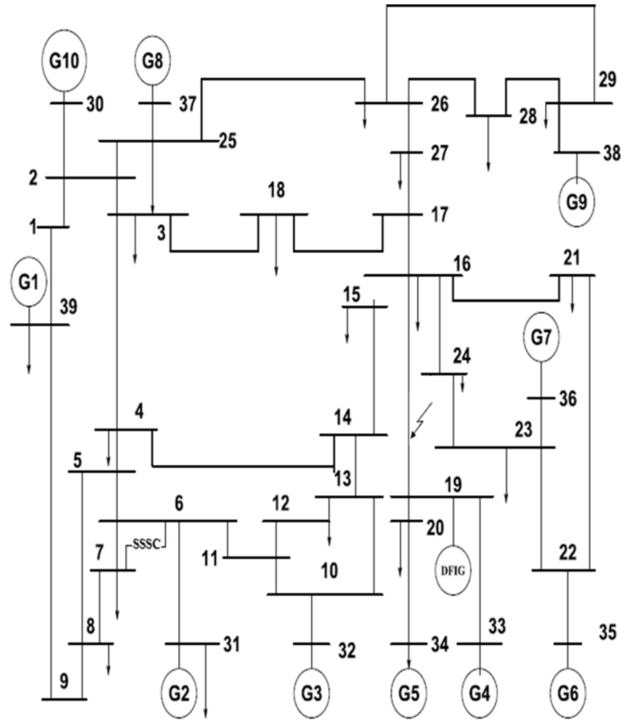

Fig. 5 The NEW ENGLAND standard 39-Bus power system which includes DFIG and SSSC.

In Figure 6-a, the speed deviations are shown. In terms of speed change, this generator has the highest speed change compared to other system generators which is about [-5, 5] rad/sec at an angular speed of 377 rad/sec, and it can change the frequency to 0.9 Hz. Linear controllers certainly cannot be used to improve stability due to extreme changes in the operating point. In the second stage, DFIG control input, and synchronous generators are considered for stability improvements by the terminal sliding mode scheme.

All simulation is cariad out based on $a_2 = 0.5$ .In Figures 6-b and 6-c, the deviations in internal angle and speed of machines after the short-circuit fault are depicted. It is clear that all the machines plus DFIG are returned to their equilibrium conditions.

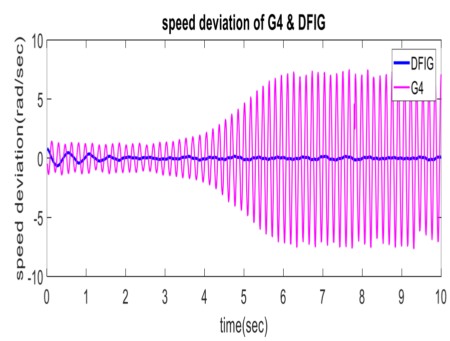

Fig. 6-a Speed deviation of G4 and DFIG without control.

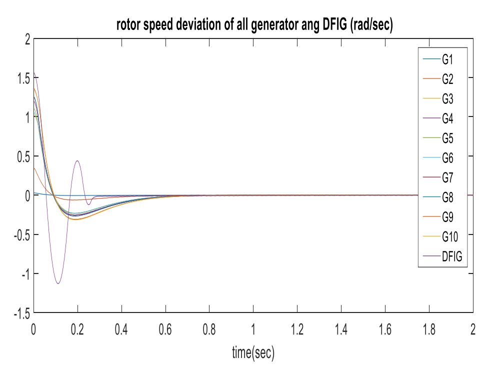

Fig. 6-b Rotor speed deviation of all generators and DFIG applying the proposed controller.

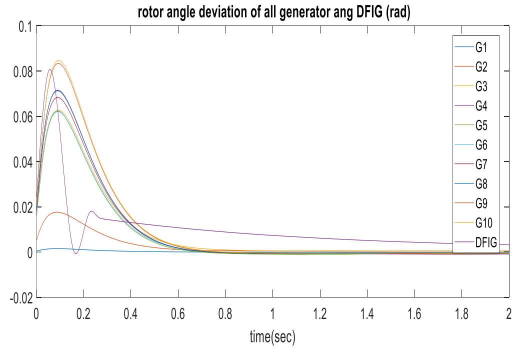

Fig. 6-c Rotor angle deviation of all generators and DFIG applying the proposed controller.

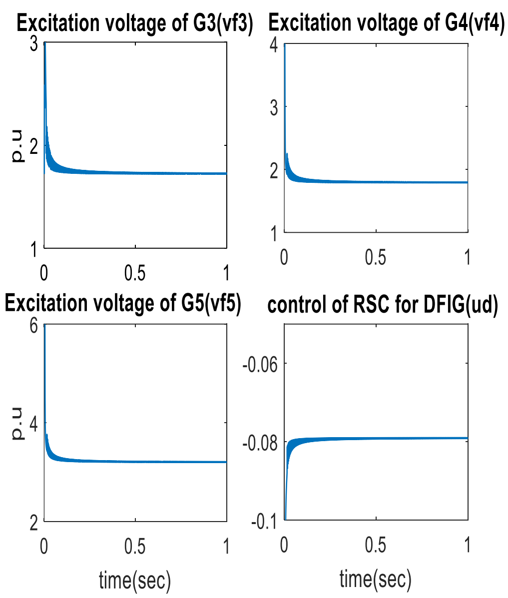

Fig. 7. Excitation voltage of G3, G4, G5, and RSC control of DFIG.

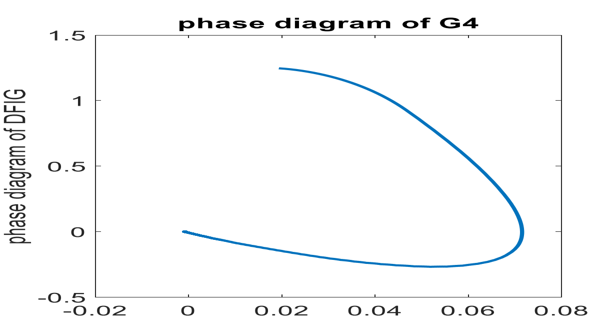

Fig. 8. The phase diagram of the G4 generator after removing the fault

In Figure (7), the excitation voltages of generators No. 3, No.4, No.5, and the control signal of DFIG are drawn due to their proximity to the fault location and greater effectiveness .For a better understanding of the phase diagrams G4 and DFIG after removing the fault are plotted in Figs. 8 and 9.

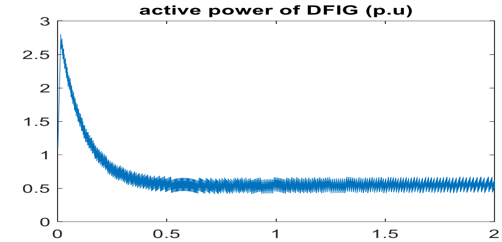

Fig. 10. Changes in the active power of DFIG after clearing the fault.

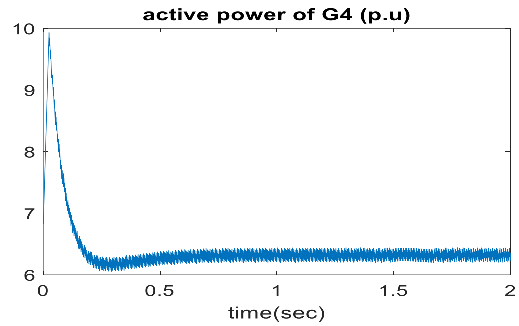

Fig. 11. Changes in the active power of the G4 generator after clearing the fault.

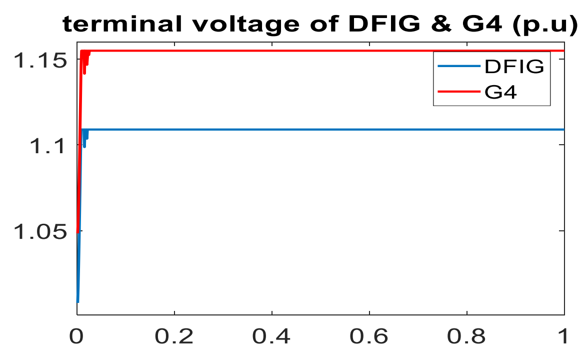

Fig. 12. Terminal voltages of G4 generator and DFIG after clearing the fault.

It is evident from the figures that the mentioned variables tend toward zero with an acceptable speed from their initial conditions after clearing the fault occurrence.

Fig. 10 and Fig. 11 depict the deviation of one of the important parameters of stability, that is, the changes in the active power for the G4 generator and DFIG. Due to the increase of the power angle during the fault, the power changes are instantaneous, and their duration is very short. After fault clearing, the controller should properly dampen these changes.

It is observed from the figures that the active powers converge to their reference values in 0.3 seconds after the fault. In Fig. 12, the plot of terminal voltages related to the G4 generator and DFIG are shown. This figure shows that the terminal voltages reach their initial values in a short duration of time after the fault occurrence.

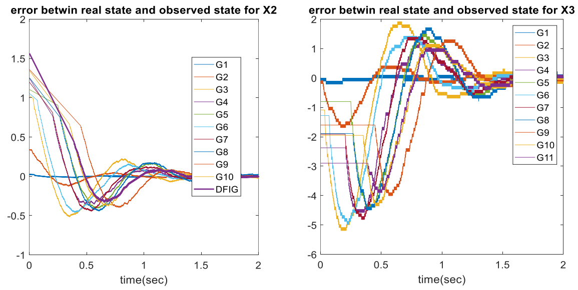

Fig. 13. The Error between the actual values and the observed values for X2 and X3 in all the generators and DFIG.

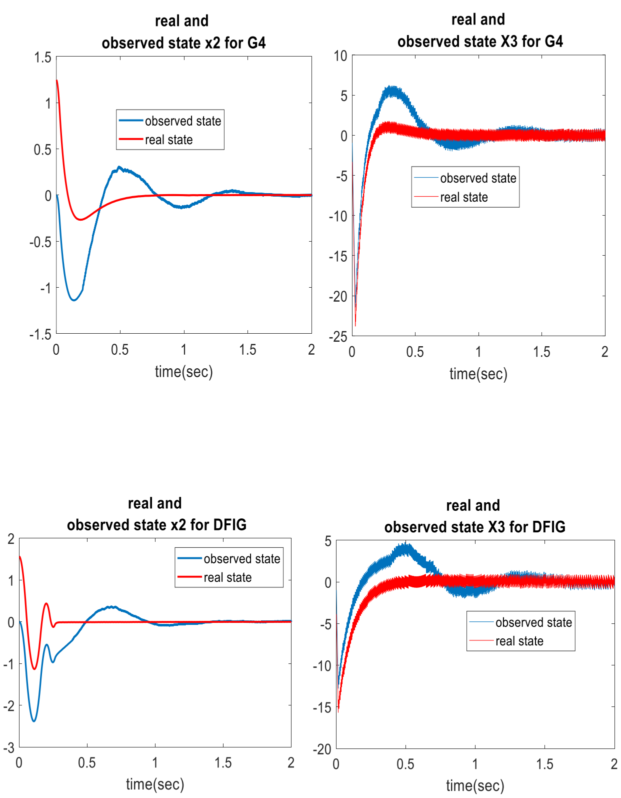

Fig. 14. A Comparison between the real state values with the observed ones for the G4 generator and DFIG.

To examine the performance of the sliding mode observer, the errors between the actual and the observed state variables x2 and x3 are plotted in Fig. 13.

The corresponding observer error reaches zero in about 2 seconds. In Fig. 14, a comparison is made between the actual states with their observed values for the G4 generator and DFIG. The figure shows that the DFIG state-variable tends to its actual value in a short duration of time.

In the following scenarios, the robustness of the designed control method against the sudden change of the mechanical power input of one of the generation units and the change of the fault location and the change of the wind speed, as the input of the DFIG have been investigated separately.

In Fig. 15, the performance of the G4 generator in the case of

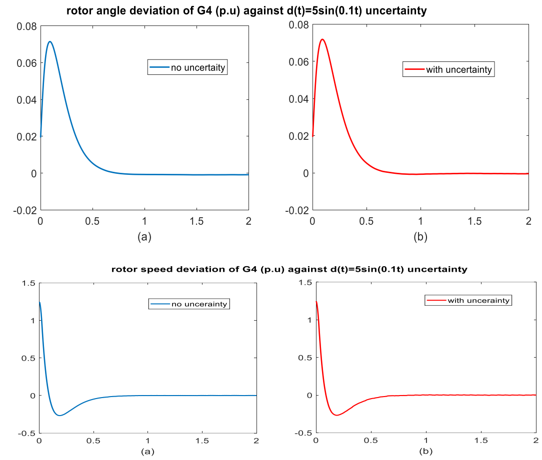

Fig. 15. A Comparison between the real state values with the observed Ones for the G4 generator and DFIG under the effect of noise.

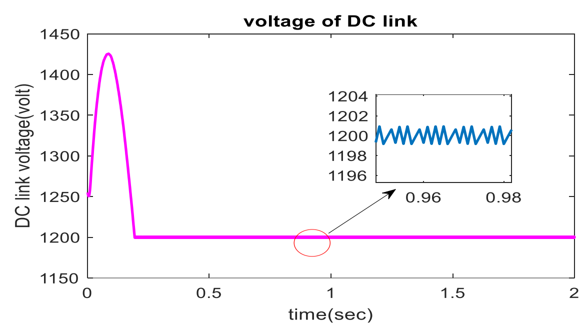

Fig. 16. Voltage of DC link in DFIG.

imposing uncertainty with the value of $d(t) = 10sin(.1t)$ to the power system is depicted. The plot shows that adding this uncertainty does not have a particularly important effect on the controller performance and the resulting output states. This fact demonstrates the robustness of the proposed control scheme, compared to the terminal sliding mode control law to structure uncertainty in the form of additional noises.

Figure (16) shows the voltage changes in the dc link of the grid-side converter. According to the figure, it can be seen that the controller designed for the grid-side converter has been able to adjust the voltage to the desired value of pre-fault.

To demonstrate the efficiency of the designed controller and its robustness to the location of the fault occurring, a short-circuit fault occurred for 100 milliseconds on bus No. 22 near generator No. 6. In Figure 17, the angular speed changes for generators No. 6 and No. 7, which are closer to the fault, are shown. According to these figures, both generators become stable after a short period of time and the controller has performed well against the fault.

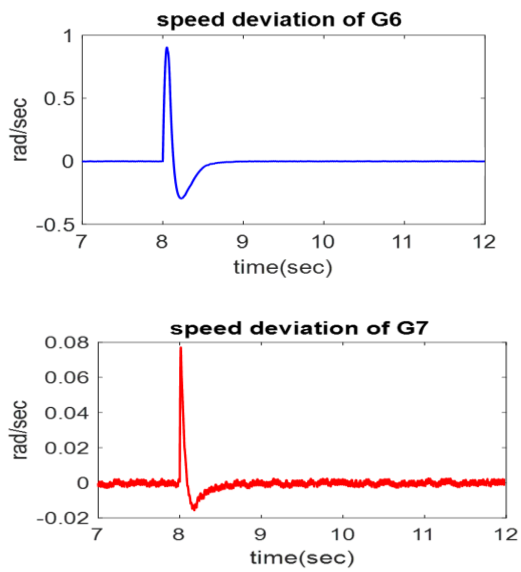

Fig. 17. Speed deviation of G6 and G7 against occurring fault at Bus No. 22.

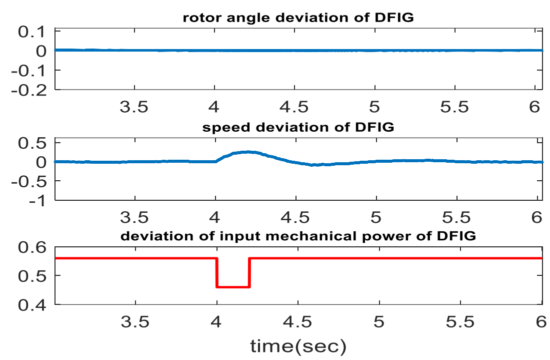

Fig. 18. Speed deviation and rotor angle deviation of DFIG against input mechanical power.

Also, considering that changes in wind speed cause changes in the input mechanical power to the DFIG generator, therefore, Figure 18 shows the changes in the angular speed and the internal voltage angle of the DFIG against a decrease in the input mechanical power by 17% in a period of 200 milliseconds. According to this figure, it can be seen that the controller performs well, the angular velocity changes are damped within 1.5 seconds and the DFIG becomes stable.

In order to further investigate, the performance of the proposed control law, with respect to the other important methods presented in the literature, a comparison is made with those in [11] and [16]. Table 2 shows the comparison in terms of overshoot, rise-time, and settling time resulting from the applied control law in the presented approach with the multi-input back-stepping method [16]. This table clearly shows the superiority of the proposed control law with respect to [16].

TABLE 2: A COMPARISON OF CONTROL CHARACTERISTICS BETWEEN THE PROPOSED APPROACH WITH [16].

	Proposed control law in this article			Nonlinear control design reported in [16]		
G3	Rise time (Sec.)	Settling time (Sec.)	Overshoot (p.u.)	Rise time (Sec.)	Settling time (Sec.)	Overshoot (p.u.)
Speed deviation	0.35	2.5	0.0015	0.5	5.0	0.005
Rotor angle	0.35	2.7	3°	0.1	5.0	15°
Control signal	0.50	2.2	0.5	0.4	7.5	3.2

TABLE 3: A COMPARISON OF CONTROL CHARACTERISTICS BETWEEN THE PROPOSED APPROACH WITH [11].

	Proposed control law in this article			Optimized linear control design reported in [11]		
G4	Rise time (Sec.)	Settling time (Sec.)	Overshoot (p.u.)	Rise time (Sec.)	Settling time (Sec.)	Overshoot (p.u.)
Speed deviation	0.28	2.3	0.0025	0.20	4.5	0.015
Rotor angle	0.30	2.5	5°	0.15	4.0	25°
Control signal	0.04	2.1	1.25	–	–	–

Table 3 demonstrates the results obtained by applying the proposed control law in this paper in comparison with the offered linear method in Ref. [11]. This table also shows the improvement in the stability characteristics with respect to the results of Ref. [11].

IX. Conclusion

In this study, a nonlinear control law based on the theory of terminal sliding modes is developed for power systems that include DFIG and SSSC. The main contribution of the paper is to enhance power system stability and to design a controller to achieve a robust closed-loop performance. A sliding mode observer is also designed to provide information on inaccessible state variables.

In the simulation results section, the 39-bus power system including DFIG and SSSC was considered, which becomes unstable by taking into account the mentioned disturbance and no controller. In the next step the system is stabilized by applying the sliding non-linear controller. The changes in the excitation field voltage of the generators and the changes in the DC link of the DFIG were shown considering the limitations on the inputs. In the next step, the effectiveness of the observer in estimating states and their convergence in the minimum possible time was shown. Next, the robustness of the designed control method against the sudden change in mechanical change of one of the generators and the changing fault location and the change of the wind speed as the input of the DFIG was investigated separately and the effectiveness of the proposed control approach was shown. In the end, this method was compared with the linear controller and the non-linear back-stepping controller, based on some control criteria that are given in Tables 2 and 3, which indicate the superiority of the proposed controller over other methods.

For instance, according to the simulation results, in Table 3, the overshot level is decreased by 40% and the settling time is decreased by 15% compared to the existing nonlinear control laws.

Appendix A:

The injected model of SSSC:

In order to model SSSC in the power system, it is assumed that SSSC is located between bus *i* and bus *j* as shown in Fig. A1. The proposed model of the SSSC is a series converter. This converter can stabilize the voltage of the power system buses and improve dynamic stability by injecting reactive power into the series branch [33].

The main goal of SSSC control approach aims to improve dynamic stability by injecting the appropriate series voltage, i.e. V_{se}. Hence, this controllable voltage of the converter can be represented by Fig. A.2.

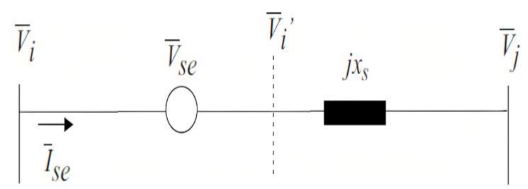

(a)

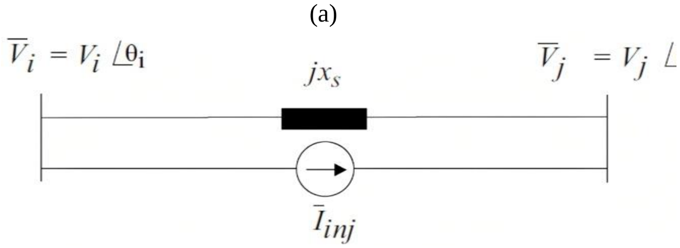

(b)

Fig. A.1. a) simplified model of SSSC, between bus *i* and bus *j*, b) equivalent circuit of SSSC.

$$\begin{cases} \dot{\delta}_i = \frac{1}{E_i' T_{oi}'}[\acute{T}_{oi}(\omega_i - \omega_s)E_i' - \\ \frac{X_i - X_i'}{X_i'} V_i \sin(\delta_i - \theta_i) + T_{oi}'\omega_s V_{ri} \cos(\delta_i - \varphi_{ri})] \\ \dot{\omega}_i = \frac{1}{M_i}[P_{mi}\frac{\omega_s}{\omega_i} - \frac{E_i' V_i^2 \sin(\delta_i - \theta_i)}{X_i'}] \\ \dot{E}_i' = \frac{1}{T_{oi}'}[\frac{X_i}{X_i'}E_i' - \frac{X_i - X_i'}{X_i'} V_i \cos(\delta_i - \theta_i)) \\ +T_{oi}'\omega_s V_{ri} \sin(\delta_i - \varphi_{ri})] \end{cases} \qquad \text{(A-1)}$$

where, V and θ are the amplitude and phase angle of the bus voltages, respectively. X_i' is the seires reactance of the system between the i-th DFIG and the bus connected to it. E_i' is the internal voltage of the i-th generator, and V_{ri} and Φ_{ri} are the amplitude and angle of the voltage applied to the DFIG rotor in polar coordinates, respectively.

From Fig.A.1 obtained:

$$\begin{cases} \bar{I}_{inj} = -jB_{ij}V_{se} \\ v_{se} = V_{se}e^{j\Phi_{se}} \\ B_{ij} = \frac{1}{x_{sij}} \end{cases} \qquad \text{(A-2)}$$

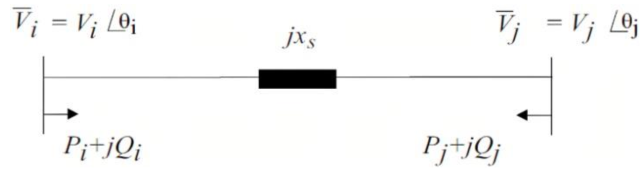

Fig. A.2. Alternative equivalent injected model of SSSC in power system.

In Fig. A.2, P_{si}, P_{sj}, Q_{si}, and Q_{sj} are defined between bus *i-th* and bus *j-th* as follows:

$$\begin{cases} S_{si} = P_{si} + jQ_{si} = -B_{ij}V_{sek}V_i \sin(\theta_i - \Phi_{sek}) \\ \quad +jB_{ij}V_{sek}V_i \cos(\theta_i - \Phi_{sek}) \\ S_{sj} = P_{sj} + jQ_{sj} = B_{ij}V_{sek}V_j \sin(\theta_j - \Phi_{sek}) \\ \quad -jB_{ij}V_{sek}V_j \cos(\theta_j - \Phi_{sek}) \end{cases} \qquad \text{(A-3)}$$

Here it is assumed that the SSSC component only generates and consumes reactive powerand also the series resistance of the transmission line on which the SSSC is located equals zero. Hence, the SSSC voltage angle is determined as follows:

$$\Phi_{sek} = tan^{-1}\left(\frac{V_j \sin(\theta_j) - V_i \sin(\theta_i)}{-V_j \cos(\theta_j) + V_i \cos(\theta_i)}\right) \qquad \text{(A-4)}$$

Modeling of DFIG used in wind energy production

Fig. 1-b demonstrates the schematic diagram of a wind generator equipped with DFIG. the equivalent with the definition of $u_{df2i} = V_{ri}sin(\Phi_{ri})$ and $u_{df1i} = V_{ri}cos(\Phi_{ri})$ after the state-space equations can be rewritten as in Eq. (A.5).

$$\begin{cases} \dot{\delta}_i = (\omega_i - \omega_s) - \frac{X_i - X_i'}{E_i' T_{0i} X_i'} Vsin(\delta_i - \theta_i) \\ \quad + \frac{\omega_s}{E_i'}(u_{df1i}cos(\delta_i) + u_{df2i}sin(\delta_i))] \\ \dot{\omega}_i = \frac{\omega_s}{2H_i}\left[P_{mi}\frac{\omega_s}{\omega_i} - \frac{E_i' V_i \sin(\delta_i - \theta_i)}{X_i'}\right] \\ \dot{\acute{E}}_i = \frac{1}{T_{oi}'}[-\frac{X_i}{\acute{X}_i}E_i' + \frac{X_i - X_i'}{X_i'}V_i \cos(\delta_i - \theta_i)) \\ \quad +T_{oi}'\omega_s(u_{d2i}sin(\delta_i) - u_{d1i}cos(\delta_i))] \end{cases}$$

(A-5)

Here, design principle is baed on using one of the inputs related to the rotor control in order to attain a strict feedback form.

$$(\omega_i - \omega_s) - \frac{X_i - X_i'}{X_i' E_i' T_{0i}} Vsin(\delta_i - \theta_i) + \frac{\omega_s}{E_i'}(u_{df1i}cos(\delta_i) + u_{df2i}sin(\delta_i)) = (\omega_i - \omega_{0i})$$

$$u_{d2i} = \frac{E_i'(\omega_s - \omega_{0i})}{\omega_s \sin(\delta_i)} + \frac{X_i - X_i'}{T_{0i}' \acute{\omega}_s X_i' \sin(\delta_i)} V_i \sin(\delta_i - \theta_i) - \frac{E_i' cos(\delta_i)}{sin(\delta_i)}\ u_{d1i}$$

(A.6)

where ω_{0i} is the speed rotation of the DFIG generator in the steady state. Substituting u_{df2i} in Eq. (A. 5):

By replacing u_{d2i} and defining $u_{d1i} = u_{di}$, it is finally obtained:

$$\begin{cases} \dot{\delta}_i = \frac{1}{\acute{E}_i T_{0i}} [-T_{0i}(\omega_i - \omega_0)\acute{E}_i - \frac{X_i - \acute{X}_i}{\acute{E}_{qi} T_{0i}} V_i sin(\delta_i - \theta_i) \ + T_{0i}\omega_0 u_{di} cos(\delta_i)] \\ \dot{\omega}_i = \frac{\omega_0}{2H_i}\left[P_{mi}\frac{\omega_s}{\omega_i} - B_i \acute{E}_i V_i \sin(\delta_i - \theta_i)\right] \\ \dot{\acute{E}}_i = \frac{1}{T_{0i}}\left[-\frac{X_i}{\acute{X}_i}\acute{E}_i + \frac{X_i - \acute{X}_i}{\acute{X}_i} V_i \cos(\delta_i - \theta_i) + T_{0i}\omega_0 u_{di} \sin(\delta_i)\right] \end{cases}$$

(A.7)

The dynamics of DC link capacitor:

By suitably controlling the grid-side converter, it is possible to control the amount of DC link voltage ripple and the amount of output reactive power. The following relationship can be used to obtain the dynamics of the capacitor voltage [31]:

$$C_{dc} V_{dc} \frac{dV_{dc}}{dt} = [P_r - P_g] \quad \text{(A.8)}$$

Considering the output voltage of the grid-side converter in polar coordinates as $V_g \measuredangle \Phi_g$, the output power from the grid-side converter to the generator terminal is obtained as follows:

$$P_g = \frac{V_g V_i}{x_g} \sin(\Phi_g - \theta_i) \quad \text{(A.9)}$$

$$Q_g = \frac{{V_g}^2}{x_g} - \frac{V_g V_i}{x_g} \cos(\Phi_g - \theta_i) \quad \text{(A.10)}$$

$$u_{g1} = V_g \cos(\Phi_g), u_{g2} = V_g \sin(\Phi_g) \quad \text{(A.11)}$$

$$V_g = \sqrt{{u_{g1}}^2 + {u_{g2}}^2}, \Phi_g = \text{atan}\left(\frac{u_{g2}}{u_{g1}}\right) \quad \text{(A.12)}$$

a result, the voltage dynamics of the DC link capacitor is obtained as follows:

$$\dot{V}_{dc} = \frac{1}{C_{dc} V_{dc}}\left[P_r - \frac{1}{x_g}(u_{g2} cos(\theta_i) - u_{g1} sin(\theta_i))\right] \quad (A.13)$$

Appendix B:

The specification of considered NEW ENGLAND 39-bus power system is presented here.

TABLE 4: EQUIVALENT SPECIFICATIONS OF WIND-TURBINE-BASED DFIG.

X_d	X'_d	X_q	H
2.605	0.107	0.0107	4

TABLE 5: EQUIVALENT SPECIFICATIONS OF SYNCHRONOUS GENERATORS.

No	H	Ra	$x'd$	xd	xq	$T'do$	xl
1	5.0	0	0.006	0.020	0.019	7.00	0.030
2	30.[illegible]	0	0.0697	0.295	0.282	6.56	0.035
3	35.[illegible]	0	0.0531	0.2495	0.237	5.70	0.0304
4	28.[illegible]	0	0.0526	0.166	0.670	0.62	0.440
5	26.[illegible]	0	0.132	0.670	0.620	5.40	0.054
6	34.[illegible]	0	0.050	0.254	0.241	7.30	0.0224
7	26.[illegible]	0	0.049	0.295	0.292	5.66	0.0322
8	24.[illegible]	0	0.057	0.290	0.280	6.70	0.028
9	34.[illegible]	0	0.057	0.2106	0.205	4.79	0.0298
10	42.[illegible]	0	0.031	0.100	0.069	10.2	0.0125

References

[1] S. Muller, M. Deicke & R I K W, “Doubly-fed induction generator systems for wind turbines,” IEEE Industry Applications Magazine, June 2002.

[2] R. M.Elavarasan , G.M. Shafiullah, S. k. Padmanaban, N. M. Kumar,” A Comprehensive Review on Renewable Energy Development, Challenges and Policies of leading Indian States with an International Perspective,“ IEEE Access, April 2020, vol. 8, pp. 74432 – 74457.

[3] T. Ariyarathna, N. Kularatna,K. Gunawardane , D. Jayananda, D. A. S. Ross, ” Development of Supercapacitor Technology and Its Potential Impact on New Power Converter Techniques for Renewable Energy, “ IEEE journal of emerging and selected topics in industrial electronics, July 2021, vol. 2, no. 3, pp. 267 – 276.

[4] N. H. Khan, Y. Wang , D. Tian, R. A .Jamal, ” A Novel Modified Lightning Attachment Procedure Optimization Technique for Optimal Allocation of the FACTS Devices in Power Systems,“ IEEE Access, April 2021, vol. 9, pp. 47976 – 47997.

[5] M. A. Chitsazan, M. S. Fadali , A. M. Trzynadlowski, ” State Estimation for Large-Scale Power Systems and FACTS Devices Based on Spanning Tree Maximum Exponential Absolute Value,” Transactions on Power Systems, August 2019, vol. 35, no. 1, pp. 238 – 248.

[6] N. H. Khan ,Y. Wang ,D .Tian, R. Jamal , S. Kamel , M. Ebeed, ”Optimal Siting and Sizing of SSSC Using Modified Salp Swarm Algorithm Considering Optimal Reactive Power Dispatch Problem,” IEEE Access, April 2021, vol. 9, pp. 49249 – 49266.

[7] P. R. Sahu, P. K. Hota, S. Panda, “ Power system stability enhancement by fractional order multi input SSSC based controller employing whale optimization algorithm,” Science Direct, Journal of Electrical Systems and Information Technology, December 2018, vol. 5, no. 3, pp. 326-336.

[8] A. Movahedi, A. Halvaei Niasar, G. Gharehpetian, "

Designing SSSC, TCSC, and STATCOM controllers using AVURPSO, GSA, and GA for transient stability improvement of a multi-machine power and GA for transient stability improvement of a multi-machine power system with PV and wind farms system with PV and wind farms," Elsevier, Electrical Power and Energy Systems, March 2019, Vol. 106 , pp. 455–466.

[9] B. K. Dubey , N. K. Singh, " Multi machine power system stability enhancement with UPFC using linear quadratic regulator techniques," International Journal of Advanced Research in Engineering and Technology , April 2020, vol. 11, pp. 219-229.

[10] M. R. Shakarami; A. Asadi Ghyasvand, A. Kazemi, " Evaluation of effect of SSSC stabilizer in different control channels on sub-synchronous resonance oscillations," Scientia Iranica, vol. 25, no. 3, pp. 1492-1506.

[11] M. Maleki, S. Abazari, " Stability Improvement of Power System With Simulation and Coordinated Control of DFIG and UPFC using LMI," International Journal of Industrial Electronics, Control and Optimization, July 2021, vol. 4, no. 3, pp. 341-353.

[12] M. A. Mahmud, "An alternative LQR-based excitation controller design for power systems to enhance small-signal stability," Int. J. Elect. Power Energy Syst, Dec. 2014, vol. 63, pp. 1–7.

[13] A. A. Vali, S. M. H. Hosseini, J. Olamaei, ''Control of doubly-fed induction generator with extended state observer under unbalanced grid conditions," Scientia Iranica, Oct 2020, vol. 29, no 5, pp. 2498-2514.

[14] S. Shojaeain, J. Soltani, Gh. Arab, ''Damping of Low Frequency Oscillations of Multi-Machine Multi-UPFC Power Systems, Based on Adaptive Input-Output Feedback Linearization Control,'' IEEE Transaction on Power Systems, May 2012, vol. 27, no. 4, pp. 1831 - 1840

[15] M. J. Morshed, A. Fekih, "A Coordinated Controller Design for DFIG-Based Multi-Machine Power Systems," IEEE systems journal, September 2019, vol. 13, no. 3, pp. 3211 - 3222

[16] T. K. Roy, M. A. Mahmud, Amanullah M. T. Oo, " Robust Adaptive Back stepping Excitation Controller Design for Higher-Order Models of Synchronous Generators in Multi machine Power Systems," IEEE Transactions on Power Systems, September 2018, vol. 34, no. 1, pp. 40 – 51.

[17] H. Wu, X. Wang , "A Mode-Adaptive Power-Angle Control Method for Transient Stability Enhancement of Virtual Synchronous Generators,", IEEE journal of emerging and selected topics in power electronics, june 2020, vol. 8, no. 2, pp. 1034 – 1049.

[18] H. S. Saravia, H. P. Painemal, D. A. Schoenwald, W. Ju," Adaptive Coordination of Damping Controllers for Enhanced Power System Stability," IEEE Open Access Journal of Power and Energy, July 2020, vol. 7, pp. 265 – 275.

[19] Y. Mi, Y. Song, Y. Fu, Ch. Wang, " The Adaptive Sliding Mode Reactive Power Control Strategy for Wind-Diesel Power System Based on Sliding Mode Observer, " Transactions on Sustainable Energy, November 2019, vol. 11, no. 4, pp. 2241 – 2251.

[20] WEI Zhang, Shizen Li, Yanju Liu, "Adaptive Sliding Mode Back-Stepping Speed Control of Hydraulic Motor for Wave Energy Conversion Device", IEEE power & energy society section, May 2020, vol. 8, pp. 89757 – 89767

[21] S. Abazari, Z. Faramarzi, " A Novel Control to Improve Dynamic Stability of Power Systems Including DFIG and SSSC," International Journal of Industrial Electronics, Control and Optimization, vol. 5, Issue 4 , December 2022, , pp. 327-336.

[22] S. Ghaedi, S. Abazari, G. R.Arab, "Novel non-linear control of DFIG and UPFC for transient stability increment of power system," IET Generation, Transmission & Distribution, vol. 16, Issue 19,October 2022, pp. 3799-4026.

[23] Z. Faramarzi, S. Abazari, S. Hoghoughi and N. R. Abjadi,"Improving the stability of the DFIG power system in the presence of SSSC in a nonlinear manner," Computational Intelligence in Electrical Engineering,vol. 14, Issue 1, May 2023, Pages 45-58.

[24] A. R. Bergen,*Power Systems Analysis*, Preticed Hall, Newjersy, 2000.

[25] Kundur, *Power System Stability and Control*, New York, USA: McGraw-Hill, 1994.

[26] K. Elkington, V. Knazkins, M. Ghandhari, "On the stability of power systems containing doubly fed induction generator-based generation," Elsevier, Electric Power Systems Research, September 2008, vol. 78, no. 9 , pp. 1477–1484.

[27] M. Noroozian, M. Ghandehari, "Improving Power System s By Series-Connected FACTS Device," IEEE Transactions on Power Delivery, October 1997, vol. 12, no. 4, pp. 1635 – 1641.

[28]Y. Feng, X. Yub, F. Han," On nonsingular terminal sliding-mode control of nonlinear systems" Elsevier, Automatica, June 2013. vol. 49, no. 6, pp. 1715-1722.

[29] V. Behnamgol, A. R. Vali, "Terminal Sliding Mode Control for Nonlinear Systems with Both Matched and Unmatched Uncertainties," Iranian Journal of Electrical & Electronic Engineering, June 2015, vol. 11, no. 2, pp. 109-117

[30] W. Perruquetti, J. P. Barbot, "Sliding Mode Conrol in Engineering", Marcel Dekker INC, New York, USA: Basel, 2002.

[31] H. Rios, R. Franco, A. F.d.Loza, D. Efimov, "A High-Order Sliding-Mode Adaptive Observer for Uncertain Nonlinear Systems," IEEE Transaction on Automatic Control, December2021,Early Access :DOI: 0.1109/TAC.2021.3139308.

[32] L. Vetoshkin, Z. K. Muller, '' Stability Improvement of Power System by Means of STATCOM With Virtual Inertia,'' IEEE ACSSES, August 2021, vol. 9, pp. 116105 – 116114.

[33] Z. Faramarzi, S. Abazari, S. Hoghoughi and N. R. Abjadi, " Dynamic stability improvement of power system with DFIG using multi-input backstepping control," Electrical Engineering, pp. 4491–4507, September 2022.

Saeed Abazari Received his BS degree in electrical engineering from Esfahan university in 1989, the MSc degree from Ferdowsi university, Mashhad, Iran In 1992, and the PhD degree from Sharif university, Tehran, Iran in 2002. He is working at the university of Shahrekord as an associated professor in electrical engineering Department. His research interests are electrical power distribution system, smart grid, and protection.